



Three-step random phase retrieval approach based on difference map normalization and diamond diagonal vector normalization

YU ZHANG,^{1,2,*} XIAOBO TIAN,³ AND RONGGUANG LIANG³

¹*Institute of Materials Physics, College of Science, Northeast Electric Power University, Jilin, Jilin 132012, China*

²*State Key Laboratory of Applied Optics, Changchun Institute of Optics, Fine Mechanics and Physics, Chinese Academy of Sciences, Changchun, Jilin 130022, China*

³*College of Optical Sciences, University of Arizona, Tucson, Arizona 85721, USA*

*521zhangyu2008@163.com

Abstract: To overcome the phase shift error in phase shifting interferometry, a three-step random phase retrieval approach based on difference map normalization and diamond diagonal vector normalization (DN&DDVN) is proposed. It does not need pre-filtering for the interferograms and can obtain relatively accurate phase distribution with a simple process and less computational time. This simulation and experiment verify the correctness and feasibility of DN&DDVN.

© 2018 Optical Society of America under the terms of the [OSA Open Access Publishing Agreement](#)

1. Introduction

Interferometry is the industry standard metrology method for optical measurement [1]. The phase shifting interferometer (PSI) was introduced by Brunning [2] to achieve accurate metrology in 1974, PSI and its variations have been widely used in optical measurement [1,3,4]. For the standard phase shifting algorithm (PSA), the phase shift between each interferogram should be a special constant (e.g. $\pi/2$), the measurement accuracy depends on the accuracy of the phase shift [4–6]. However, the practical phase shift often deviates from the pre-set value because of the error caused by the miscalibration of piezo-transducer (PZT), vibrational error, air turbulence in the working environment, instability of the laser frequency, and so on [7–9].

In order to overcome the phase shift error, two types of random PSAs have been proposed. The first type is the iterative method which can obtain the phase distribution and unknown phase shift from a series of phase shifted interferograms. These iterative methods typically consume a lot of computational time. In 2004, an advanced iterative algorithm (AIA) based on a least-squares iterative procedure was introduced to extract phase distribution from randomly phase shifted interferograms [10]. It copes with the limitation of the existing iterative algorithms by separating a frame-to-frame iteration from a pixel-to-pixel iteration, and provides stable convergence and accurate phase extraction even when the phase shifts are completely random. In 2008, Xu et al. [11] presented an advance iterative algorithm to extract phase distribution from randomly and spatially non-uniform phase shifted interferograms, this algorithm divides the interferograms into small blocks and retrieves local phase shifts accurately by iterations. In 2013, an iterative PSA based on the least-squares principle was developed to overcome the random piston and tilt wavefront errors generated from the phase shifter [12].

The second type is non-iterative random PSA. The accuracy may be not as high as the iteration methods, but it spends less time to extract the tested phase distribution. In [13], Farrell and Player utilized Lissajous figures and ellipse fitting to calculate the phase difference between two interferograms, but it needs pre-filtering and the correction result is not accurate if the intensity distribution is non-uniform. In [14], Liu et al. proposed a PSA

which can simultaneously extract the tested phase and phase shift from only two interferograms using Lissajous figure and ellipse fitting technology, however, the two interferograms used in this algorithm also need to be filtered by the Hilbert-Huang pre-filtering, and the non-uniform intensity distribution also affects the accuracy. From 2003 to 2014, Cai et al. [15–23] proposed a series of statistical algorithms which can extract the phase shifts and tested phase, however, most of these algorithms need to know the intensities of object and reference [24–30]. proposed a series of PSAs based on principal component analysis (PCA), which can fast and easily extract the phase distribution from randomly phase shifted interferograms. The PCA is an efficient technique for phase extraction by converting a set of possibly correlated variables into a set of values of uncorrelated variables, but it cannot determine the global sign of the measured phase, and it needs more than three interferograms because it need to subtract relatively accurate mean [31]. presented a two-step demodulation based on the Gram-Schmidt orthonormalization method (GS2), where phase shift is random and can be any value inside the range $[0, 2\pi]$ except π , it requires subtracting the DC term by filtering before performing GS2 [32]. proposed an advanced GS method called GS3, the major advantage of this method is that it performs well when the phase shift is close to π as most two-step algorithms become invalid in this situation. For the above non-iterative methods, most of them need pre-filtering or subtracting the mean of all the interferograms to subtract the background intensity, they need more time and may introduce extra error. To save time and increase the accuracy, the research of non-iterative methods without pre-filtering is essential.

Recently, we proposed a random two-step PSA based on Lissajous ellipse fitting and least squares technologies [33], this algorithm uses only two interferograms to extract the relatively accurate tested phase distribution and unknown phase shift without pre-filtering, and it can be used in the non-uniform background intensity and modulation amplitude. However, the Lissajous ellipse fitting and least squares technologies are time consuming.

To achieve the high measurement accuracy with less time, the PSA is critical as well. For non-iterative random PSAs with less than 3 phase shifted interferograms, it is difficult to obtain the high accurate phase distribution with less time because of the pre-filtering or the DC term subtraction.

In this paper, we will discuss the effective and accurate three-step phase retrieval approach with unknown phase shift. Section 2 presents the principle and process of the proposed PSA based on difference map normalization and diamond diagonal vector normalization (DN&DDVN). In Section 3 the simulation of DN&DDVN is discussed, and the comparison with GS2, PCA and AIA is performed. Section 4 evaluates the novel algorithm with the experimental data. The conclusion is finally drawn in Section 5.

2. Principles

In PSI, three phase shifted interferograms with total pixels of K can be described as:

$$\begin{aligned} I_{1k} &= a_k + b_k \cos(\varphi_k + \theta_1) \\ I_{2k} &= a_k + b_k \cos(\varphi_k + \theta_2) \\ I_{3k} &= a_k + b_k \cos(\varphi_k + \theta_3) \end{aligned} \quad (1)$$

where $k = 1, 2, \dots, K$ denotes the pixel position, I_{1k} , I_{2k} and I_{3k} are the intensity of three interferograms, a_k and b_k respectively represent the background intensity and modulation amplitude, φ_k is the tested phase, and θ_1 , θ_2 and θ_3 are the phase shifts. Because there is only a piton θ_1 between φ_k and $\varphi_k + \theta_1$, which doesn't affect the phase distribution, for simplicity, we define $\theta_1 = 0$ in the following discussion.

In order to filter the background intensity, we implement the subtraction between the three phase shifted interferograms. Thus, two difference maps between the first, second, and third interferograms can be defined as:

$$D_{1k} = I_{1k} - I_{2k} = 2b_k \sin\left(\frac{\theta_2}{2}\right) \sin\left(\varphi_k + \frac{\theta_2}{2}\right) = 2b_k \sin\left(\frac{\theta_2}{2}\right) \cos\left(\Phi_k - \frac{\pi}{2}\right) = 2b_k \sin\left(\frac{\theta_2}{2}\right) \cos(\Phi'_k) \quad (2)$$

$$D_{2k} = I_{1k} - I_{3k} = 2b_k \sin\left(\frac{\theta_3}{2}\right) \sin\left(\varphi_k + \frac{\theta_3}{2}\right) = 2b_k \sin\left(\frac{\theta_3}{2}\right) \cos\left(\Phi_k + \Delta - \frac{\pi}{2}\right) = 2b_k \sin\left(\frac{\theta_3}{2}\right) \cos(\Phi'_k + \Delta) \quad (3)$$

where $\Phi_k = \varphi_k + \frac{\theta_2}{2}$, $\Delta = \frac{\theta_3 - \theta_2}{2}$, $\Phi'_k = \Phi_k - \frac{\pi}{2}$.

Since the phase shifts between the different interferograms are different, $\theta_2 \neq \theta_3$ and $2b_k \sin\left(\frac{\theta_2}{2}\right) \neq 2b_k \sin\left(\frac{\theta_3}{2}\right)$, the amplitude of D_{1k} is different from D_{2k} . Hence, to eliminate the effect of the different amplitudes, the normalization is introduced to cope with two difference maps.

Generally, the normalization of the vector u can be expressed as:

$$u^* = u / \sqrt{\langle u, u \rangle} = u / \|u\| \quad (4)$$

where u^* represents the normalized vector, $\|\cdot\|$ and $\langle \cdot, \cdot \rangle$ respectively represent the 2-norm and the inner product.

Normalizing the two difference vectors D_{1k} and D_{2k} , we can obtain:

$$D_{1k}^* = \frac{D_{1k}}{\|D_{1k}\|} = \frac{b_k \cos(\Phi'_k)}{\sqrt{\sum_{k=1}^K b_k^2 \cos^2(\Phi'_k)}} \quad (5)$$

$$D_{2k}^* = \frac{D_{2k}}{\|D_{2k}\|} = \frac{b_k \cos(\Phi'_k + \Delta)}{\sqrt{\sum_{k=1}^K b_k^2 \cos^2(\Phi'_k + \Delta)}} \quad (6)$$

If we have more than one fringe in the interferograms, we can use the approximation:

$$\sqrt{\sum_{k=1}^K b_k^2 \cos^2(\Phi'_k)} \approx \sqrt{\sum_{k=1}^K b_k^2 \cos^2(\Phi'_k + \Delta)} \quad (7)$$

Then the above normalized difference vectors can be rewritten as:

$$D_{1k}^* = c_k \cos(\Phi'_k) \quad (8)$$

$$D_{2k}^* = c_k \cos(\Phi'_k + \Delta) \quad (9)$$

$$\text{where } c_k = \frac{b_k}{\sqrt{\sum_{k=1}^K b_k^2 \cos^2(\Phi'_k)}} = \frac{b_k}{\sqrt{\sum_{k=1}^K b_k^2 \cos^2(\Phi'_k + \Delta)}}$$

We can see that the proposed method is invalid if $\Delta = 0$, however θ_2 cannot be equal to θ_3 since the phase shift must exist between different phase shifted interferograms, hence the above normalization is unrestricted except for more than one fringe is needed in the interferogram.

From Eqs. (8) and (9), we can see that the normalized difference vectors D_{1k}^* and D_{2k}^* are just as two phase shifted interference signals without the background intensity. Hence, we can use the two-step PSA to extract the phase distribution easily.

In the following, we use a two-step algorithm based on the diamond diagonal vector normalization (DDVN). D_{1k}^* and D_{2k}^* are two corresponding vectors with the same length but different directions, they constitute the adjacent sides of a diamond, in which the diagonals are perpendicular and can be geometrically defined as the sum and difference of them respectively. Hence, two orthogonal DDV are presented by:

$$\hat{D}_{dif} = D_{1k}^* - D_{2k}^* = 2c_k \sin\left(\Phi'_k + \frac{\Delta}{2}\right) \sin \frac{\Delta}{2} \quad (10)$$

$$\hat{D}_{sum} = D_{1k}^* + D_{2k}^* = 2c_k \cos\left(\Phi'_k + \frac{\Delta}{2}\right) \cos \frac{\Delta}{2} \quad (11)$$

Figure 1 shows the geometrical relationship between two normalized difference vectors D_{1k}^* , D_{2k}^* , and the corresponding diagonal vectors. In general, $2c_k \sin \frac{\Delta}{2} \neq 2c_k \cos \frac{\Delta}{2}$ except $\Delta = \pi/2$ or $3\pi/2$, hence the amplitude of \hat{D}_{dif} is also different from \hat{D}_{sum} . It is necessary to perform the normalization again.

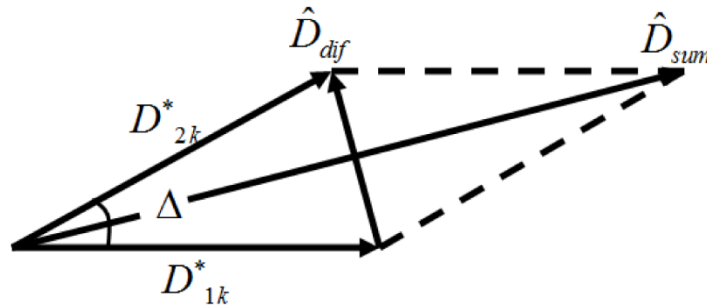


Fig. 1. Geometrical relationship between two normalized vectors D_{1k}^* , D_{2k}^* and the corresponding diagonal vectors.

Normalizing two orthogonal DDV, we can get:

$$\tilde{D}_{dif} = \frac{c_k \sin\left(\Phi'_k + \frac{\Delta}{2}\right)}{\sqrt{\sum_{k=1}^K c_k^2 \sin^2\left(\Phi'_k + \frac{\Delta}{2}\right)}} \quad (12)$$

$$\tilde{D}_{sum} = \frac{c_k \cos\left(\Phi'_k + \frac{\Delta}{2}\right)}{\sqrt{\sum_{k=1}^K c_k^2 \cos^2\left(\Phi'_k + \frac{\Delta}{2}\right)}} \quad (13)$$

when there is more than one fringe,

$$\sqrt{\sum_{k=1}^K c_k^2 \sin^2\left(\Phi'_k + \frac{\Delta}{2}\right)} \approx \sqrt{\sum_{k=1}^K c_k^2 \cos^2\left(\Phi'_k + \frac{\Delta}{2}\right)} \quad (14)$$

Equations (12) and (13) can be simplified as:

$$\tilde{D}_{dif} = d_k \sin\left(\Phi'_k + \frac{\Delta}{2}\right) \quad (15)$$

$$\tilde{D}_{sum} = d_k \cos\left(\Phi'_k + \frac{\Delta}{2}\right) \quad (16)$$

where $d_k = \frac{c_k}{\sqrt{\sum_{k=1}^K c_k^2 \sin^2\left(\Phi'_k + \frac{\Delta}{2}\right)}} = \frac{c_k}{\sqrt{\sum_{k=1}^K c_k^2 \cos^2\left(\Phi'_k + \frac{\Delta}{2}\right)}}$. Finally, according to Eqs. (15)

and (16), we can get:

$$\Phi'_k = \arctan\left(\frac{\tilde{D}_{dif}}{\tilde{D}_{sum}}\right) - \frac{\Delta}{2} \quad (17)$$

The tested phase can be determined by:

$$\Phi_k'' = \Phi'_k + \frac{\Delta}{2} = \arctan\left(\frac{\tilde{D}_{dif}}{\tilde{D}_{sum}}\right) \quad (18)$$

We know that there is only a piston between φ_k and Φ_k'' , which doesn't affect the phase distribution, hence we can use Φ_k'' to express the tested phase distribution.

From Eq. (2) to Eq. (9), we can see that the background intensity and modulation amplitude inconsistency have been nearly eliminated through normalizing the difference maps. Two-step PSA based on the DDVN can be performed to rapidly obtain the tested phase. Importantly, the phase with high accuracy can be achieved with random phase shift.

3. Simulation

To validate the effectiveness and robustness of the proposed method, we perform simulations with non-uniform background intensity and modulation amplitude. Simple circular fringes, different numbers of phase shifted fringe patterns, different phase shifts, different levels of noises and complex fringes will be studied in the simulations.

In the first simulation, we assume that:

$$\begin{aligned} a &= 1.3 \exp\left[-0.02(x^2 + y^2)\right], b = 1.2 \exp\left[-0.02(x^2 + y^2)\right] \\ \varphi &= 5\pi(x^2 + y^2), \theta_1 = 0rad, \theta_2 = 1rad, \theta_3 = 3rad \end{aligned} \quad (19)$$

where $-1 \leq x \leq 1, -1 \leq y \leq 1$. To verify the validity of the approximations from Eqs. (7) and (14), we perform the calculation using the simulated data from Eq. (19). Through the calculation, for Eq. (7), $\sqrt{\sum_{k=1}^K b^2_k \cos^2(\Phi'_k)}$ which is 338.5817 is approximately equal to $\sqrt{\sum_{k=1}^K b^2_k \cos^2(\Phi'_k + \Delta)}$ which is 336.9096, and for Eq. (14), $\sqrt{\sum_{k=1}^K c^2_k \sin^2\left(\Phi'_k + \frac{\Delta}{2}\right)}$ and $\sqrt{\sum_{k=1}^K c^2_k \cos^2\left(\Phi'_k + \frac{\Delta}{2}\right)}$ are respectively 0.9807 and 1.0025, they are also approximately equal, hence, the approximations from Eqs. (7) and (14) can be recognized effective. According to Eq. (19), three phase shifted interferograms with size 401*401 are generated, in addition we add 20dB Gauss noise generated by the function awgn in Matlab to the interferograms, as shown in Figs. 2(a)-2(c). The simulated background intensity, modulation amplitude, and theoretical phase distribution ($PV = 31.416$ rad, $RMS = 6.656$ rad) are shown in Figs. 2(d)-2(f).

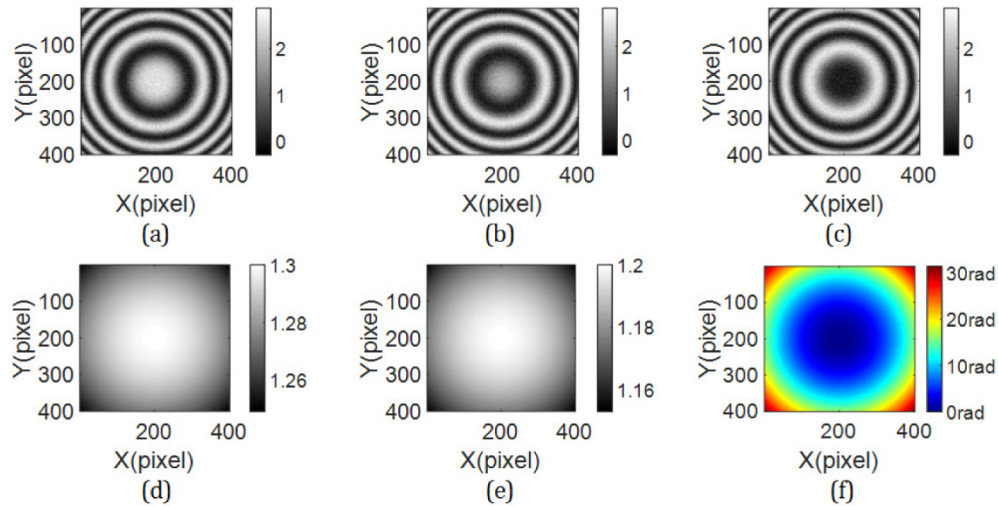


Fig. 2. Simulated interferograms, background intensity, modulation amplitude and phase distribution. (a), (b) and (c) the three phase shifted interferograms, (d), (e) and (f) the simulated background intensity, modulation amplitude, and theoretical phase distribution.

In order to verify the performance of the proposed method, we compare it with GS3, PCA and AIA. For AIA, the initial phase shifts are respectively set as 0, 0.5 and 1 rad. Figures 3(a)-3(d) show the phase distributions using DN&DDVN, GS3, PCA and AIA, the differences are not obvious, but can be identified from the phase error distributions as shown in Figs. 3(e)-3(h). Table 1 shows the RMS phase errors and computational time of the different methods. The RMS phase error from GS3 is nearly 2 times the other three methods. For DN&DDVN, PCA, and AIA, the accuracy of AIA is highest, but the computational time is also longest due to the iterations, in addition its accuracy and computational time depend on the initial values and iterative times. For PCA, the RMS phase error of PCA is a little larger than DN&DDVN, and the computational time is also a little longer than DN&DDVN due to the PCA process, in addition it needs extra process to determine the global sign of the measured phase, further increasing the computational complexity and time. Only for DN&DDVN, it can balance the accuracy and computational time, it can be seen that, it has least computational time and relative high accuracy.

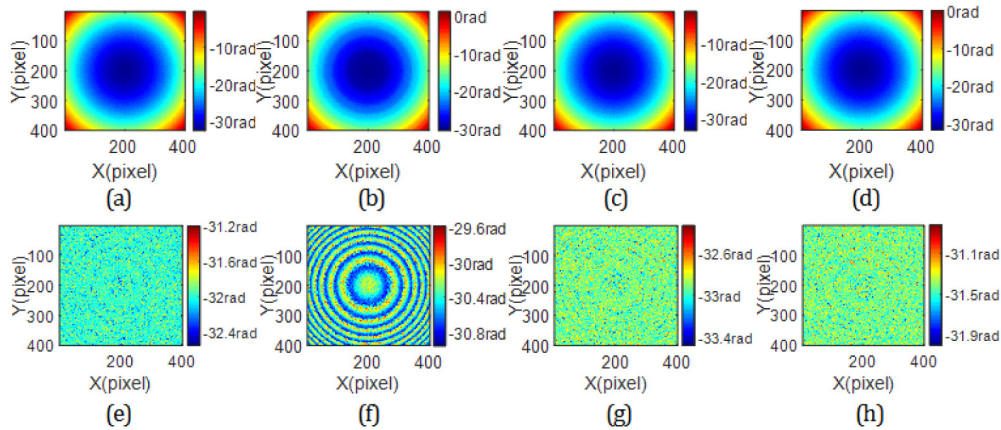


Fig. 3. Simulated results. (a), (b), (c), and (d) the extracted phase distributions using DN&DDVN (RMS = 6.658 rad), GS3 (RMS = 6.667 rad), PCA (RMS = 6.657 rad), and AIA (RMS = 6.658 rad), (e), (f), (g), and (h) the phase error distributions after using DN&DDVN, GS3, PCA, and AIA.

Table 1. RMS phase errors and computational time of the different methods

Method	DN&DDVN	GS3	PCA	AIA
RMS phase error (rad)	0.1039	0.2308	0.1044	0.1032
Time (s)	2.20	2.21	2.31	19.13

In the second simulation, provided that the tested phase distribution $\varphi = k\pi(x^2 + y^2)$, which k represents the number of the phase shifted fringe patterns in one interferogram. In Section 2, in order to obtain the accurate phase distribution, we assume that there is more than one fringe in the interferogram, in the following, we vary the number of the phase shifted fringe patterns while fixing the SNR to 20dB to obtain the range of the fringe numbers using DN&DDVN. As can be seen from Table 2, when the fringe number is less than 0.7, the RMS phase error is relative larger, and the ratio of RMS phase to RMS phase error is less than 10 (In general, the ratio of RMS phase to RMS phase error is more than 10 in the accurate measurement). For the range of fringe numbers between 0.8 and 1.2, the RMS phase error is unstable. When the range of fringe numbers is between 1.3 and 2.0, the ratio is increasing with the increase of fringe number, and the RMS phase error is decreasing with the increase of fringe number, that is to say, the approximation error from Eq. (7) and Eq. (14) is decreasing with the increase of fringe number. When the number of patterns is more than 2, the RMS phase errors are similar, in this case, the approximation error is nearly stable, hence, we can conclude that the number of patterns is best to be more than 2 if high accuracy is requested.

Table 2. RMS phase and RMS phase errors with different numbers of the phase shifted fringe patterns using DN&DDVN

Patterns	0.5	0.6	0.7	0.8	0.9	1.0	1.1	1.2
RMS Phase (rad)	0.6656	0.7987	0.9319	1.0650	1.1981	1.3312	1.4643	1.5975
RMS phase error (rad)	0.1916	0.1436	0.1192	0.1102	0.1086	0.1101	0.1132	0.1147
Patterns	1.3	1.4	1.5	1.6	1.7	1.8	1.9	2.0
RMS Phase (rad)	1.7306	1.8637	1.9968	2.1300	2.2631	2.3962	2.5293	2.6625
RMS phase error (rad)	0.1156	0.1133	0.1103	0.1077	0.1058	0.1052	0.1051	0.1055
Patterns	3.0	4.0	5.0	15	25	35	45	
RMS Phase (rad)	3.9937	5.3249	6.6561	19.9684	33.2807	46.5929	59.9052	
RMS phase error (rad)	0.1046	0.1043	0.1042	0.1042	0.1039	0.1038	0.1039	

In the third simulation, the phase shifts of the first and second frames are respectively set as 0 and 0.7 rad while the phase shift of the third frame is changed from 1.7 rad to 3.84 rad (the range of relative phase shift between the second and third interferograms is from 1 rad to

3.14 rad). As shown in Table 3, the relationship between the RMS phase error and phase shift is presented. Obviously, it can be seen that, while the phase shift is lower than 2 rad, the RMS phase error is significantly larger than that when the phase shift is larger than 2 rad since small practical phase shift $(\theta_3 - \theta_2)/2$ will introduce large phase error. Moreover, the RMS phase error decreases with the increase of the phase shift value, the nearer the practical phase shift $(\theta_3 - \theta_2)/2$ approximates to $\pi/2$, the smaller the RMS phase error is. As described in [34], in the case that the phase shift is larger than 2.5 rad, almost all two-step PSAs do not work well, but DN&DDVN could solve this problem. In addition, the relative phase shift cannot be set as π in most two-step PSAs, the simulation shows that DN&DDVN can remove this restriction.

Table 3. RMS phase errors with different phase shifts using DN&DDVN method

Phase shift (rad)	1.700	1.844	1.988	2.132	2.276	2.420
RMS phase error (rad)	0.4995	0.2132	0.1928	0.1781	0.1657	0.1574
Phase shift (rad)	2.564	2.708	2.852	2.996	3.140	3.840
RMS phase error (rad)	0.1489	0.1435	0.1387	0.1350	0.1325	0.1320

In the fourth simulation, we design five phase shifted fringe patterns with different levels of noises. Table 4 shows the extracted RMS phase errors of different methods as the SNR of noise increases from 20 dB to 70dB. As can be seen from Table 4, for all the methods the larger the noise, the larger the RMS phase error. Moreover, the phase error of GS3 is larger than other methods even when the noise is relatively small or no noise since the inherent error of GS3 is relatively large. We plot the RMS phase errors for the different levels of noises except GS3 as shown in Fig. 4, the phase errors are relatively small when the SNR of noise is more than 50dB. From Table 4, we can see that, when there is no noise in the interferograms, the phase error still exists for all the methods due to the non-uniform background intensity or inherent errors of them. At last, we simulate the situation with uniform background intensity and no noise, only the RMS phase error of AIA is close to 0, that is to say, the AIA doesn't have the inherent error, the DN&DDVN, GS3 and PCA all have the inherent errors since they all have the approximation, however, for DN&DDVN and PCA, the phase error can be ignored when the noise is relative small. If the high measurement accuracy is required, we can use DN&DDVN or PCA firstly, then using the extracted phase distribution as the initial value of AIA to calculate the final phase distribution, the inherent errors can be eliminated finally, however the computational time will be extended.

Table 4. RMS phase errors and processing time with different levels of noises using different methods

SNR	20dB	30 dB	40 dB	50 dB	60 dB	70 dB	No noise	Uniform background
DN&DDVN	0.1042	0.0336	0.0131	0.0087	0.0081	0.0081	0.0081	0.0078
GS3	0.2310	0.2106	0.2085	0.2083	0.2083	0.2083	0.2083	0.2083
PCA	0.1045	0.0498	0.0175	0.0094	0.0082	0.0081	0.0081	0.0078
AIA	0.1038	0.0327	0.0104	0.0035	0.0015	0.0012	0.0011	9.7259e-4

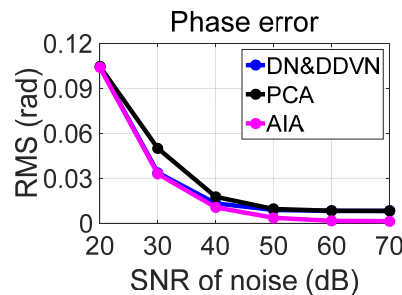


Fig. 4. RMS phase errors of different methods with different levels of noises.

In the last simulation, we simulate the complex fringes and compare the proposed method with GS3, PCA and AIA as the first simulation in order to verify the robustness of DN&DDVN. The given phase distribution is set as the complex wavefront:

$$\varphi = 5\pi(x^2 + y^2 + x^3 + y^3) + 10 \text{peaks}(401) - \langle 5\pi(x^2 + y^2 + x^3 + y^3) + 10 \text{peaks}(401) \rangle \quad (20)$$

where we use the function *peaks* in Matlab, and $\langle \cdot \rangle$ is the average operator. Other conditions are same as the previous simulations. One of the complex interferograms is shown in Fig. 5 (a), it can be seen that the fringes are the asymmetrical complex fringes. The extracted phase distribution (Fig. 5(b)) using DN&DDVN (RMS = 22.307 rad) is almost the same as the reference phase distribution (RMS = 22.307 rad) as shown in Fig. 5(c). RMS phase error is 0.1037 rad, same order of the magnitude as the circular fringes discussed above, and the phase error distribution is shown in Fig. 5(d). Moreover, the compared results are shown in Table 5, we can get the same conclusion as the above simple fringes from Table 5, hence, we can get the conclusion that, the proposed method is valid for both the simple and complex fringes.

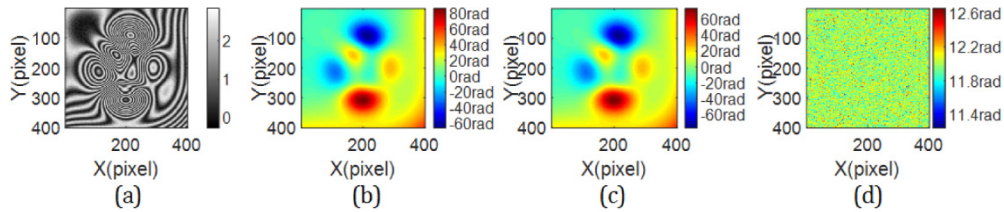


Fig. 5. Simulated results of complex fringes using DN&DDVN. (a) One of the simulated complex interferograms, (b), (c) and (d) the reference phase distribution, extracted phase distribution, and phase error distribution.

Table 5. RMS phase errors and computational time of the different methods for complex fringes

Method	DN&DDVN	GS3	PCA	AIA
RMS phase error (rad)	0.1037	0.3284	0.1042	0.1034
Time (s)	2.29	2.36	2.45	19.54

Based on the above different simulations, the advantages of the proposed DN&DDVN can be summarized as: 1) It can balance the accuracy and computational time; 2) it can obtain the tested phase distribution by only the DN&DDVN process without the pre-filtering and global sign determination as PCA; 3) the phase shift can be random, and the proposed method removes the restriction that the relative phase shift cannot be set as π in most two-step PSAs; 4) the measurement accuracy and speed of DN&DDVN are irrelevant to the numbers of the fringe patterns; and 5) whether the simple or complex fringes, the proposed method is valid.

4. Demonstration with experimental data

Optical experiments have also been carried out to investigate the performance of our method. Three phase shifted interferograms with circular fringes are collected to perform the phase retrieval by the proposed DN&DDVN, GS3 and PCA. The extracted phase using AIA with correctly initial phase shifts and 10 iterations is set as the reference phase, in this situation, the accuracy of AIA is relatively high. The size of the interferograms is 301*301, and the phase shifts are 0, $\pi/2$ and π . One of the interferograms is shown in Fig. 6(a), the extracted phase distributions using DN&DDVN, GS3 and PCA are plotted in Figs. 6(b)-6(d), Fig. 6(e) shows the reference phase distribution. The differences between the reference phase and the phase obtained by DN&DDVN, GS3 and PCA are shown in Fig. 7, and the RMS values are respectively 0.0145 rad, 0.3035 rad and 0.0141rad, further indicating that the accuracy of phase retrieval with DN&DDVN and PCA is indeed higher than that with GS3. In addition,

the computational time of different methods are shown in Table 6, we can see that, DN&DDVN has the least computational time, and AIA has the longest computational time.

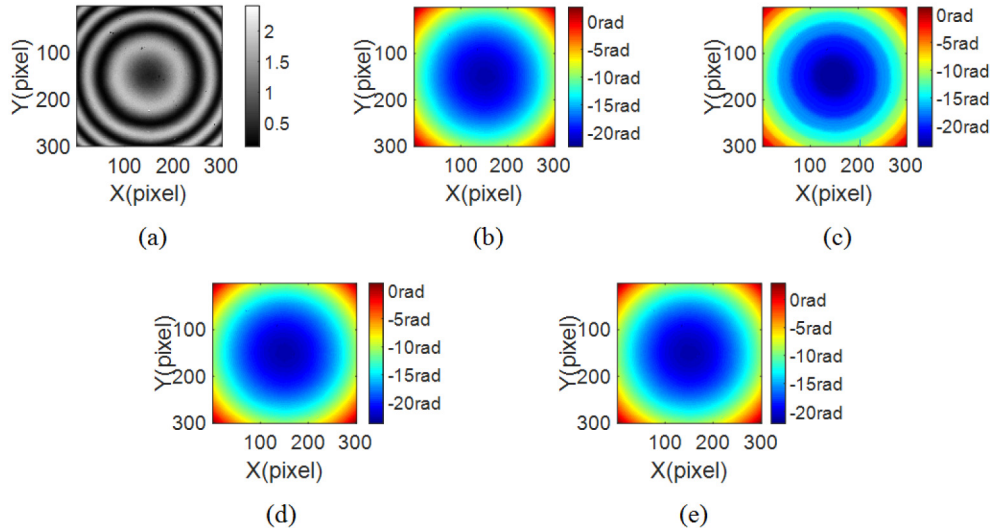


Fig. 6. Experimental results of the circular fringes. (a) One of the phase shifted interferograms, (b), (c), and (d) the extracted phase distributions obtained by DN&DDVN (RMS = 5.0283 rad), GS3 (RMS = 5.0525 rad) and PCA (RMS = 5.0284 rad), (e) the reference phase distribution obtained by AIA (RMS = 5.0283 rad).

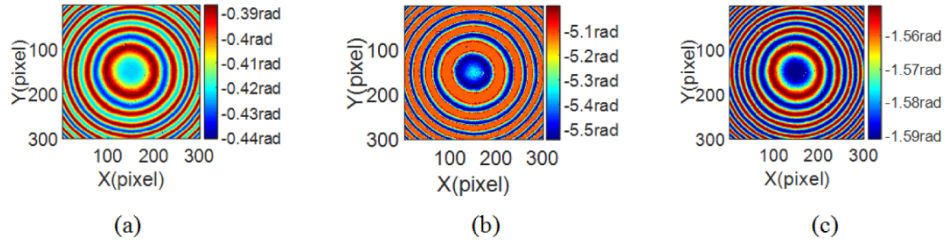


Fig. 7. The differences between the reference and extracted phase distributions for circular fringes: (a) DN&DDVN, (b) GS3, and (c) PCA.

Table 6. Computational time of the different methods for circular fringes

Method	DN&DDVN	GS3	PCA	AIA
Time (s)	1.78	1.83	1.85	10.91

To verify the robustness of DN&DDVN, the phase shifted interferograms with complex fringes are also collected, and the comparison for different methods are performed as the circular fringes. The size of the interferograms is 201*201, and the phase shifts are also 0, $\pi/2$ and π . Figure 8 show one of the phase shifted interferograms, and the extracted phase distributions using different methods, the extracted phase distribution using AIA is also set as the reference phase distribution. Figure 9 show the differences between the reference phase and extracted phase by DN&DDVN, GS3 and PCA, the RMS values are respectively 0.0252 rad, 0.2883 rad and 0.0252 rad, we can see that the accuracy of phase retrieval with DN&DDVN and PCA is also higher than that with GS3 for complex fringes. For the computational time, which are shown in Table 7, we get the conclusion the same as the circular fringes. Through the above experiments, we verify that, for both the simple and complex fringes, the proposed DN&DDVN without pre-filtering can obtain relatively accurate result with less computational time by only three interferograms.

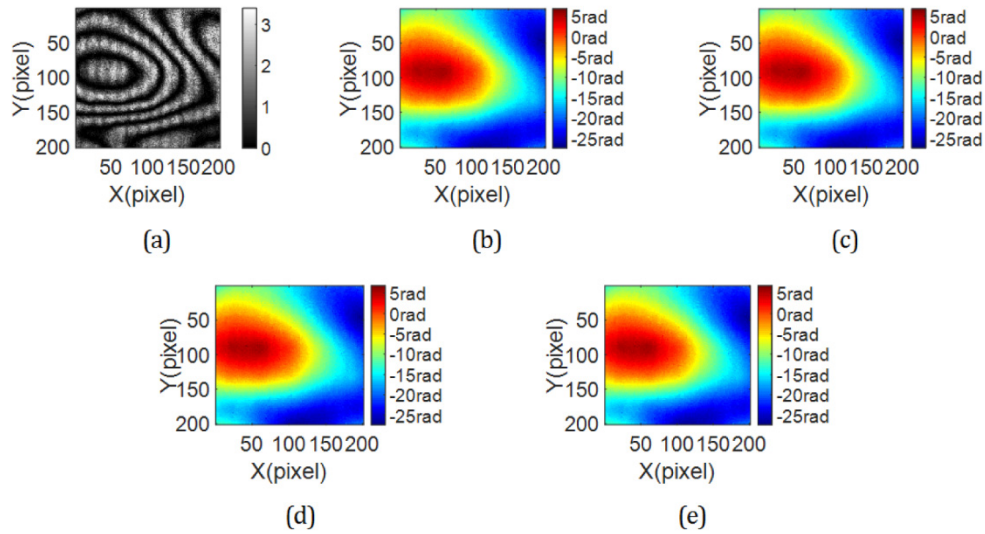


Fig. 8. Experimental results of the complex fringes. (a) One of the phase shifted interferograms, (b), (c), and (d) the extracted phase distributions obtained by DN&DDVN (RMS = 8.8850 rad), GS3 (RMS = 8.8925 rad) and PCA (RMS = 8.8850 rad), (e) the reference phase distribution obtained by AIA (RMS = 8.8851 rad).

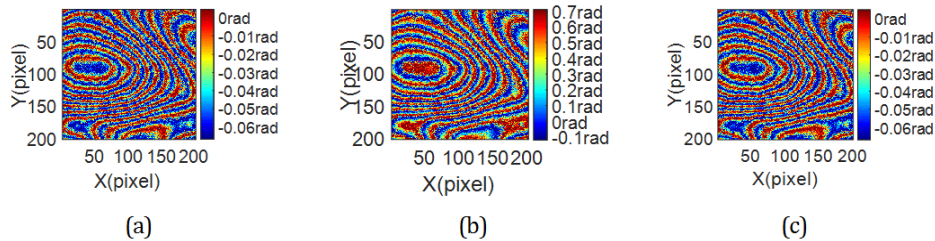


Fig. 9. The differences between the reference and extracted phase distributions for complex fringes: (a) DN&DDVN, (b) GS3, and (c) PCA.

Table 7. Computational time of the different methods for complex fringes

Method	DN&DDVN	GS3	PCA	AIA
Time (s)	1.06	1.09	1.15	6.76

5. Conclusion

In this paper, we present a random three-step phase retrieval approach based on DN&DDVN, the difference maps are obtained by three phase shifted interferograms firstly, and then normalization is performed for the difference maps. Next the sum and difference of the normalized difference maps, which can be seen as the diagonal vectors of the diamond, are computed and the normalization is performed again to obtain the tested phase distribution. We have compared this proposed method with GS3, PCA and AIA by the simulated data and experimental data. The proposed method can achieve high accuracy without pre-filtering and global sign determination, and it can directly obtain the tested phase with less computational time. In addition, it removes the restriction that the relative phase shift cannot be set as π in most two-step PSAs. Last but not least, it is robust for both the simple and complex fringes with the non-uniform background intensity and modulation amplitude.

Funding

National Natural Science Foundation of China (NSFC) (11304034); Program of China Scholarship Council (201508220104); Program of Jilin Provincial Educational Department

(2015241); State Key Laboratory of Applied Optics; Doctoral Research Foundation of Northeast Electric Power University (BSJXM-201218); Scientific Basic Research Foundation of Northeast Electric Power University.

References

1. D. Malacara, *Optical Shop Testing*, 3rd ed. (John Wiley & Sons, Inc., 2007), Chap. 1–7.
2. J. H. Bruning, D. R. Herriott, J. E. Gallagher, D. P. Rosenfeld, A. D. White, and D. J. Brangaccio, “Digital wavefront measuring interferometer for testing optical surfaces and lenses,” *Appl. Opt.* **13**(11), 2693–2703 (1974).
3. C. Tian and S. Liu, “Two-frame phase-shifting interferometry for testing optical surfaces,” *Opt. Express* **24**(16), 18695–18708 (2016).
4. K. Kinnstaetter, A. W. Lohmann, J. Schwider, and N. Streibl, “Accuracy of phase shifting interferometry,” *Appl. Opt.* **27**(24), 5082–5089 (1988).
5. K. Hibino, B. F. Oreb, D. I. Farrant, and K. G. Larkin, “Phase-shifting algorithms for nonlinear and spatially nonuniform phase shifts,” *J. Opt. Soc. Am. A* **14**(4), 918–930 (1997).
6. M. Servin, J. C. Estrada, and J. A. Quiroga, “The general theory of phase shifting algorithms,” *Opt. Express* **17**(24), 21867–21881 (2009).
7. D. Malacara, *Optical Shop Testing*, 3rd ed. (John Wiley & Sons, Inc., 2007), Chap. 14.
8. P. J. de Groot, “Vibration in phase-shifting interferometry,” *J. Opt. Soc. Am. A* **12**(2), 354–365 (1995).
9. L. L. Deck, “Suppressing phase errors from vibration in phase-shifting interferometry,” *Appl. Opt.* **48**(20), 3948–3960 (2009).
10. Z. Wang and B. Han, “Advanced iterative algorithm for phase extraction of randomly phase-shifted interferograms,” *Opt. Lett.* **29**(14), 1671–1673 (2004).
11. J. Xu, Q. Xu, and L. Chai, “Iterative algorithm for phase extraction from interferograms with random and spatially nonuniform phase shifts,” *Appl. Opt.* **47**(3), 480–485 (2008).
12. Y. C. Chen, P. C. Lin, C. M. Lee, and C. W. Liang, “Iterative phase-shifting algorithm immune to random phase shifts and tilts,” *Appl. Opt.* **52**(14), 3381–3386 (2013).
13. C. T. Farrell and M. A. Player, “Phase step measurement and variable step algorithms in phase-shifting interferometry,” *Meas. Sci. Technol.* **3**(10), 953–958 (1992).
14. F. Liu, J. Wang, Y. Wu, F. Wu, M. Trusiak, K. Patorski, Y. Wan, Q. Chen, and X. Hou, “Simultaneous extraction of phase and phase shift from two interferograms using Lissajous figure and ellipse fitting technology with Hilbert-Huang prefiltering,” *J. Optics-UK* **18**(10), 105604 (2016).
15. L. Z. Cai, Q. Liu, X. L. Yang, and Y. R. Wang, “Sensitivity adjustable contouring by digital holography and a virtual reference wavefront,” *Opt. Commun.* **221**(1–3), 49–54 (2003).
16. L. Z. Cai, Q. Liu, and X. L. Yang, “Phase-shift extraction and wave-front reconstruction in phase-shifting interferometry with arbitrary phase steps,” *Opt. Lett.* **28**(19), 1808–1810 (2003).
17. L. Z. Cai, Q. Liu, and X. L. Yang, “Generalized phase-shifting interferometry with arbitrary unknown phase steps for diffraction objects,” *Opt. Lett.* **29**(2), 183–185 (2004).
18. X. F. Meng, L. Z. Cai, X. F. Xu, X. L. Yang, X. X. Shen, G. Y. Dong, and Y. R. Wang, “Two-step phase-shifting interferometry and its application in image encryption,” *Opt. Lett.* **31**(10), 1414–1416 (2006).
19. X. F. Xu, L. Z. Cai, X. F. Meng, G. Y. Dong, and X. X. Shen, “Fast blind extraction of arbitrary unknown phase shifts by an iterative tangent approach in generalized phase-shifting interferometry,” *Opt. Lett.* **31**(13), 1966–1968 (2006).
20. X. F. Xu, L. Z. Cai, Y. R. Wang, X. L. Yang, X. F. Meng, G. Y. Dong, X. X. Shen, and H. Zhang, “Generalized phase-shifting interferometry with arbitrary unknown phase shifts: Direct wave-front reconstruction by blind phase shift extraction and its experimental verification,” *Appl. Phys. Lett.* **90**(12), 121124 (2007).
21. X. F. Xu, L. Z. Cai, Y. R. Wang, X. F. Meng, W. J. Sun, H. Zhang, X. C. Cheng, G. Y. Dong, and X. X. Shen, “Simple direct extraction of unknown phase shift and wavefront reconstruction in generalized phase-shifting interferometry: algorithm and experiments,” *Opt. Lett.* **33**(8), 776–778 (2008).
22. X. F. Xu, L. Z. Cai, Y. R. Wang, and R. S. Yan, “Direct phase shift extraction and wavefront reconstruction in two-step generalized phase-shifting interferometry,” *J. Opt.* **12**(1), 015301 (2010).
23. R. S. Yan, L. Z. Cai, and X. F. Meng, “Correction of wave-front retrieval errors caused by the imperfect collimation of reference beam in phase-shifting interferometry,” *Optik (Stuttg.)* **125**(2), 601–605 (2014).
24. J. Vargas, J. A. Quiroga, and T. Belenguier, “Phase-shifting interferometry based on principal component analysis,” *Opt. Lett.* **36**(8), 1326–1328 (2011).
25. J. Vargas, J. A. Quiroga, and T. Belenguier, “Analysis of the principal component algorithm in phase-shifting interferometry,” *Opt. Lett.* **36**(12), 2215–2217 (2011).
26. J. Deng, K. Wang, D. Wu, X. Lv, C. Li, J. Hao, J. Qin, and W. Chen, “Advanced principal component analysis method for phase reconstruction,” *Opt. Express* **23**(9), 12222–12231 (2015).
27. J. Xu, W. Jin, L. Chai, and Q. Xu, “Phase extraction from randomly phase-shifted interferograms by combining principal component analysis and least squares method,” *Opt. Express* **19**(21), 20483–20492 (2011).
28. K. Yatabe, K. Ishikawa, and Y. Oikawa, “Improving principal component analysis based phase extraction method for phase-shifting interferometry by integrating spatial information,” *Opt. Express* **24**(20), 22881–22891 (2016).

29. K. Yatabe, K. Ishikawa, and Y. Oikawa, "Simple, flexible, and accurate phase retrieval method for generalized phase-shifting interferometry," *J. Opt. Soc. Am. A* **34**(1), 87–96 (2017).
30. K. Yatabe, K. Ishikawa, and Y. Oikawa, "Hyper ellipse fitting in subspace method for phase-shifting interferometry: Practical implementation with automatic pixel selection," *Opt. Express* **25**(23), 29401–29416 (2017).
31. J. Vargas, J. A. Quiroga, C. O. Sorzano, J. C. Estrada, and J. M. Carazo, "Two-step demodulation based on the Gram-Schmidt orthonormalization method," *Opt. Lett.* **37**(3), 443–445 (2012).
32. H. Wang, C. Luo, L. Zhong, S. Ma, and X. Lu, "Phase retrieval approach based on the normalized difference maps induced by three interferograms with unknown phase shifts," *Opt. Express* **22**(5), 5147–5154 (2014).
33. Y. Zhang, X. Tian, and R. Liang, "Random two-step phase shifting interferometry based on Lissajous ellipse fitting and least squares technologies," *Opt. Express* **26**(12), 15059–15071 (2018).
34. J. Vargas, J. A. Quiroga, C. O. Sorzano, J. C. Estrada, and J. M. Carazo, "Two-step interferometry by a regularized optical flow algorithm," *Opt. Lett.* **36**(17), 3485–3487 (2011).